Anisotropic phonon coupling in the relaxor ferroelectric $(Na_{1/2}Bi_{1/2})TiO_3$ near its high-temperature phase transition

Ling Cai and Jean Toulouse
Physics Department, Lehigh University, Bethlehem, Pennsylvania 18015, USA

Haosu Luo
Shanghai Institute of Ceramics, Chinese Academy of Science, Shanghai 201800, China

Wei Tian
Quantum Condensed Matter Division, Oak Ridge National Laboratory, Oak Ridge, Tennessee 37831, USA
(Received 1 January 2014; revised manuscript received 11 August 2014; published 28 August 2014)

The lead free relaxor $Na_{1/2}Bi_{1/2}TiO_3$ (NBT) undergoes a structural cubic-to-tetragonal transition near 800 K which is caused by the cooperative rotations of O_6 octahedra. These rotations are also accompanied by the displacements of the cations and the formation of the polar nanodomains (PNDs) that are responsible for the characteristic dielectric dispersion of relaxor ferroelectrics. Because of their intrinsic properties, spontaneous polarization, and lack of inversion symmetry, these PNDs are also piezoelectric and can mediate an interaction between polarization and strain or couple the optic and acoustic phonons. Because PNDs introduce a local tetragonal symmetry, the phonon coupling they mediate is found to be anisotropic. In this paper we present inelastic neutron scattering results on coupled transverse acoustic (TA) and transverse optic (TO) phonons in the [110] and [001] directions and across the cubic-tetragonal phase transition at $T_C \sim 800$ K. The phonon spectra are analyzed using a mode coupling model. In the [110] direction, as in other relaxors and some ferroelectric perovskites, a precipitous drop of the TO phonon into the TA branch or "waterfall" is observed at a certain $q_{\rm wf} \sim 0.14$ r.l.u. In the [001] direction, the highly overdamped line shape can be fitted with closely positioned bare mode energies which are largely overlapping along the dispersion curves. Two competing lattice coupling mechanism are proposed to explain these observations.

DOI: 10.1103/PhysRevB.90.054118 PACS number(s): 61.05.F−, 77.80.Jk, 77.65.Ly

I. INTRODUCTION

Among relaxors, NBT has recently been the subject of extensive studies due to its environmentally friendly chemical composition and high electromechanical coefficients, both characteristics that are desirable for future device applications [1–4]. Unlike the *B* site disordered $PbMg_{1/3}Nb_{2/3}O_3$ (PMN) and $PbZn_{1/3}Nb_{2/3}O_3$ (PZN), NBT and a few others are rarer cases in the relaxor family in which the substitution takes place on the *A* site. In NBT, Na^{1+} and Bi^{3+} are randomly substituted for each other in a 1:1 average ratio. Size and/or valence mismatch between substituted cations usually induces off-centering. Systems with the perovskite structure are known to exhibit one of two structural instabilities leading to phase transitions, rotations of the anion octahedra (tilting), or displacements of the cations (shifting). Tilting transitions are well known to occur in compounds such as $SrTiO_3$, $KMnF_3$, and $NaNbO_3$ [5–7] and shifting or ferroelectric transitions in $BaTiO_3$ and $PbTiO_3$, etc. NBT is a special member of the perovskite family, simultaneously exhibiting both instabilities [8,9]. Therefore, in NBT, the rotations of the O_6 octahedra appear to be coupled to certain cation displacements. In addition, the off-centered cations form local dipoles which eventually lead to the formation of nanosize polar domains (PNDs) [10,11]. It is the reorientation of these PNDs that gives rise to the characteristic low frequency dielectric dispersion in NBT [12]. In addition, because they are polar and tetragonally distorted, PNDs represent local "piezoelectric" regions within the surrounding paraelectric cubic lattice [13]. Their polarization can therefore be modulated by the soft transverse optic phonon (TO) which can thus become coupled to the transverse acoustic phonon (TA). As is shown later, the data presented can be explained by such a coherent interaction between TO and TA phonons, piezoelectrically mediated by PNDs.

NBT undergoes two structural phase transitions, a cubic-to-tetragonal transition at ∼800 K and a tetragonal-to-rhombohedral transition at ∼580 K [8]. The high temperature transition is triggered by the condensation of a soft mode (Σ_3 symmetry [5]) at the *M* point of the Brillouin zone boundary, which corresponds to the $a^0a^0c^+$ (Glazer notation [7]) tilting of the O_6 octahedra. However, this transition also coincides with the onset of the characteristic dielectric dispersion that is due to the formation of the PNDs, and the displacements of the Na/Bi and Ti cations against one another when viewed along ⟨001⟩ [8,12]. The lower temperature transition is triggered by the condensation of a soft zone boundary phonon at the *R* point, corresponding to $a^-a^-c^-$ tilting of the O_6 octahedra [8,14,15]. Concurrently, Na/Bi and Ti cations become displaced parallel to ⟨111⟩ in order to accommodate the antiphase rotation of the O_6 octahedra and a ferroelectric order is established [8,15], presumably accompanied by the alignment of the PNDs.

A commonly observed phonon anomaly in relaxor systems is the so-called "waterfall" effect. It manifests itself as a precipitous drop of the TO branch toward the acoustic branch at some finite wave vector $q_{\rm wf}$, below which the TO mode is no longer distinguishable in the spectrum. Early studies in Pb relaxors related this effect to the critical damping of the TO mode, either due to its strong interaction with PNDs of a characteristic size comparable to $1/q_{\rm wf}$ or to the presence of

strong disorder-induced random fields [16–19]. Other studies have suggested that the waterfall is the result of mode coupling between the TO and TA phonon modes [20,21]. A similar phonon dispersion anomaly was also reported by Swainson *et al.* in $Pb(Mg_{1/3}Nb_{2/3})O_3$ at the zone boundary, which was referred to as "columns" of TO mode [22]. Most recently, a waterfall behavior was reported by Matsuura *et al.* in NBT at lower temperature [3]. In spite of the large amount of literature on the waterfall effect, significant differences of opinion still persist with regard to its physical interpretation.

In the present study we report inelastic neutron scattering results of the lowest energy TA and TO phonons in the (002) and (220) Brillouin zones (BZ) from the Γ point to the zone boundary, respectively, M and X points. Phonons propagating along the two orthogonal directions ⟨110⟩ (Σ_4) and ⟨001⟩ (Δ_5) [5] were measured in constant q and constant E scans between 1000 and 700 K. These results reveal a prominent waterfall feature at small q in the (002) Brillouin zone, which can be satisfactorily described by a mode coupling model. In the [220] zone the dispersion curves do not reveal a similar waterfall effect but suggest a different coupling mechanism between the TO and TA branches. Results in the two zones are successively reported, then compared and discussed.

II. EXPERIMENTAL SETUP

A single NBT crystal about 5 × 10 × 20 mm was cut to a half dome shape out of a larger boule grown by the TSSG method. Neutron scattering measurements were performed on the HB1a triple axis spectrometer at the High Flux Isotope Reactor (HFIR), Oak Ridge National Laboratory. The sample was mounted on a tantalum sample holder in vacuum inside a furnace. The HB1A spectrometer operates with a fixed incident energy $E_i = 14.6$ meV using a double pyrolitic graphite (PG) monochromator system. A collimation of 40′-40′-sample-40′-80′ was used throughout the experiment, giving an energy resolution of 1 meV. Measurements of the phonon spectra were made in the neutron energy gain mode. Such a mode is adequate for high temperature phonon measurements, for which the energy transfer ΔE is much smaller than k_BT [23]. One set of scans was taken at room temperature and the others were taken upon cooling from 1000 down to 700 K.

The phonons were measured in the $[HHL]$ scattering plane. The scattering relationship $\mathbf{Q} = \tau_{\mathbf{hkl}} + \mathbf{q}$ holds for our inelastic scans, where $\mathbf{Q}$ is the scattering vector, $\tau_{\mathbf{hkl}}$ is a reciprocal lattice vector, and $\mathbf{q}$ is the phonon wave vector. Transverse scans were performed near the (002) and (220) Bragg reflections where the structure factors for both TA and TO phonons are large. Focusing conditions were chosen within the $(\mathbf{Q},E)$ plane by selecting negative $\mathbf{q}$ values in the (002) zone and positive $\mathbf{q}$ values in the (220) zone. In the following, pseudocubic notations are used throughout and the wave vectors are indicated in reduced lattice units ξ, where $\xi = \frac{|\mathbf{q}|}{2\pi/a}$, with $a = 3.92$ Å measured at high temperature in the cubic phase. All inelastic scans were corrected for the resolution volume effect as stipulated in Ref. [23] for fixed E_i mode; and all data were normalized to the beam monitor count.

III. RESULTS AND ANALYSIS

A. Phase transition and the [110] phonon in the (002) zone

In the measurement sequence, the (002) Bragg peak was monitored during cooling to determine the transition temperature. As seen in the inset of Fig. 1, the transition is marked by a large increase in the intensity of the Bragg peak below ∼800 K (relief of extinction). Such an intensity increase is a commonly observed phenomenon near symmetry lowering transitions. It is due to the formation of domains along different possible orientations, resulting in strains in the crystal that effectively increase its mosaicity and reduce internal back scattering. The transition temperature obtained is in good agreement with that from other diffraction studies of NBT [4,8,15]. The rather abrupt change of intensity below ∼800 K suggests a first-order-like transition. NBT undergoes another transition at lower temperature (∼580 K), which was not part of the present study.

In the (002) zone, measurements were made of the TA and TO phonons propagating in the $\mathbf{q} \parallel [110]$ direction and polarized along the $\mathbf{e} \parallel [001]$ direction (Σ_4 symmetry [5,24]). Constant q scans were made from the zone center Γ point to the zone boundary at $\xi = 0.5$. Representative spectra for different temperatures are shown in Fig. 2. Two features can immediately be noticed at the zone center in Fig. 2(a): the lack of temperature variation in the inelastic portion of the spectrum and the absence of a well-defined phonon mode up to 15 meV. At $\xi = 0.05$ in Fig. 2(b), a single peak is observed at $\Delta E \approx 2.5$ meV. Note that a strong central peak background appears to contribute to the asymmetric line shape, as shown in the inset. Figure 2(c) shows the zone boundary phonon behavior at (0.5, 0.5, 2). At this q value the TO mode is very broad and centered around ∼18 meV, whereas the TA phonon mode remains well structured and centered at ∼5 meV. The dashed line indicates the approximate position of the TA mode peak, whose energy is seen to remain relatively constant throughout the temperature range investigated.

Next, in Fig. 3 we examine the near zone center spectra at $\xi = 0.1$ and $\xi = 0.15$ and at several temperatures. The

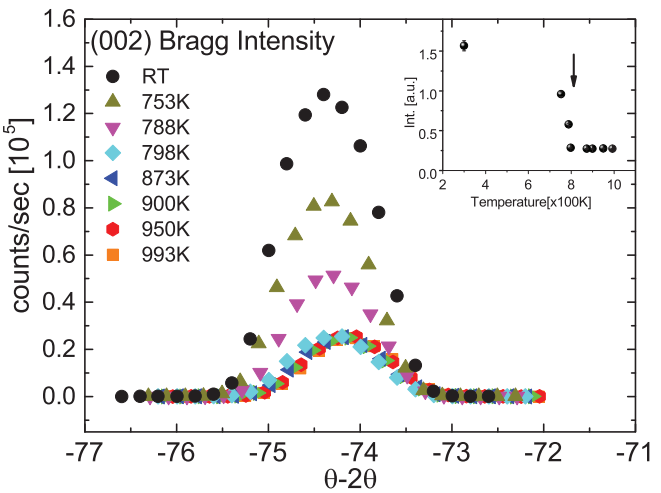

FIG. 1. (Color online) θ-2θ scan at (002) Bragg reflection measured across $T_C = 800$ K. The inset shows the sharp increase of integrated intensity at $T_C = 800$ K.

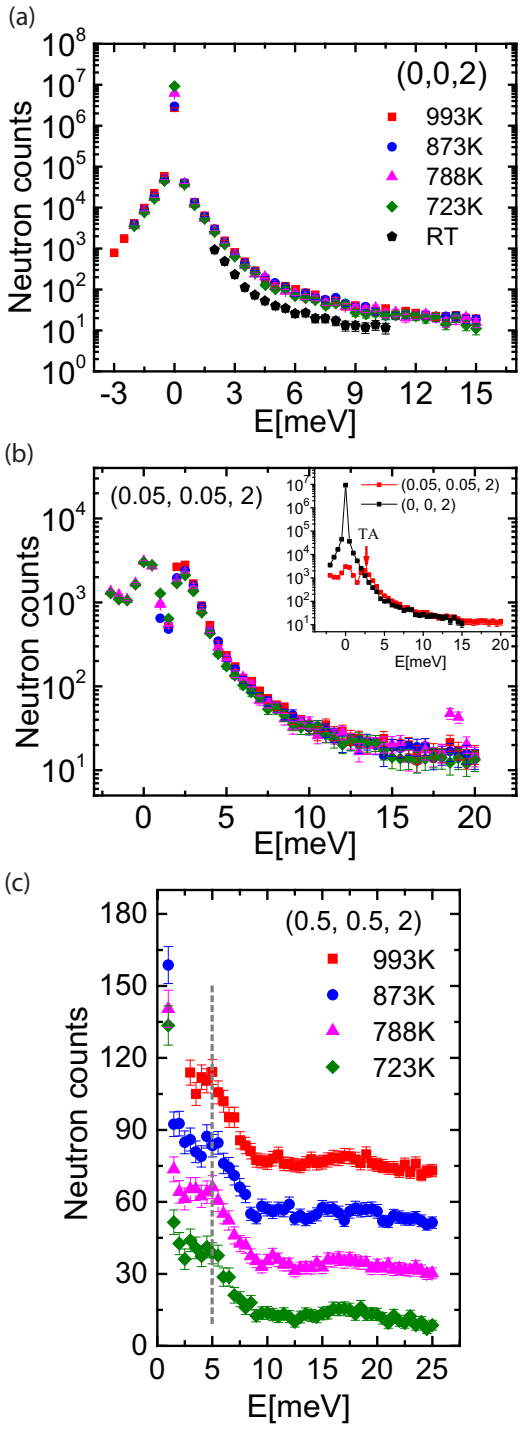

FIG. 2. (Color online) Constant q scans near (002) zone at (a) Γ point, (b) (0.05, 0.05, 2), and (c) (0.5, 0.5, 2). The inset in (b) indicates that the central peak background intensity is very high at (0.05, 0.05, 2). The spectra in (c) are offset by a constant for clarity and the dashed line is guide to the eye for the average peak position.

multitemperature plots at $\xi = 0.1$ are shown in the left column and the $\xi = 0.15$ plots in the right column. The $\xi = 0.1$ spectra show a single peak, with a possible shoulder on the high frequency side, but the $\xi = 0.15$ spectra distinctly reveal both a TA and a TO mode, particularly well resolved at room temperature. Neither set of the spectra displays a noticeable

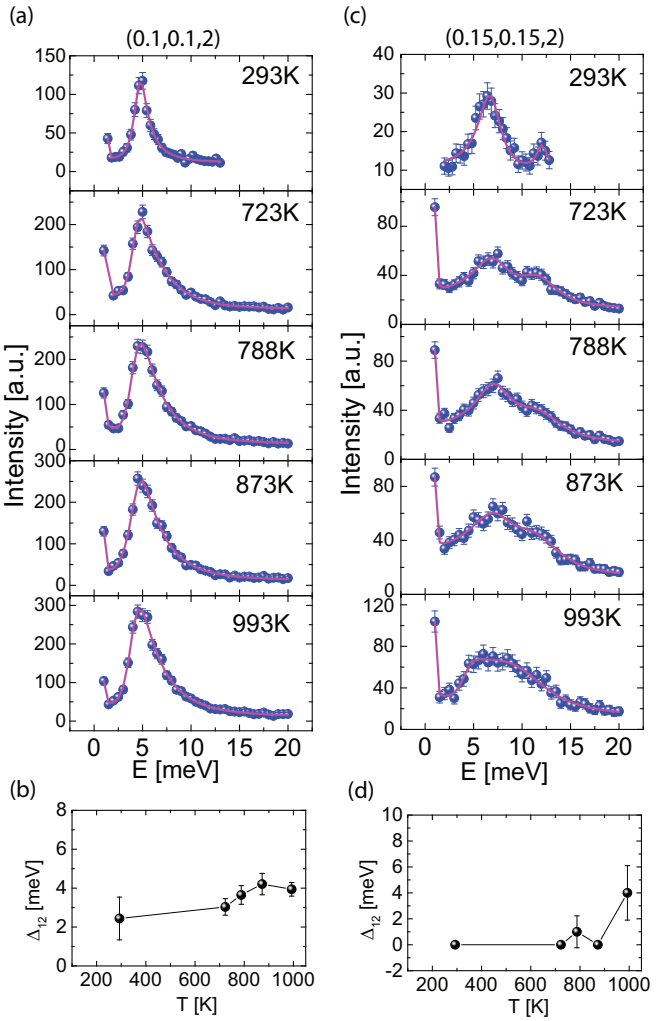

FIG. 3. (Color online) Near zone center plots of the [110] phonon fitted with mode coupling equation at (a) $\xi = 0.1$ and (c) $\xi = 0.15$. The resulting coupling constants are plotted in (b) and (d), respectively.

temperature dependence in the temperature range studied, except at room temperature. At higher temperatures however, the two modes overlap and, being of the same symmetry, must therefore be coupled. Consequently, the spectra were fitted with a mode coupling (MC) function previously used to describe the phonon interaction in perovskite systems [25–27]. It is important to note that fitting with other models such as two uncoupled damped harmonic oscillators (DHOs) was also attempted but the MC model was found to give the fastest converging and best overall fitting as well as the smallest χ^2 value. Together with a Gaussian central peak and a constant background, the scattering function can be expressed as

$$S_{\text{total}} = S_{\text{elastic}} + S_{\text{MC}} + S_{\text{bkg}},$$

in which S_{MC} takes the form

$$S_{\text{MC}}(\omega) = n(\omega)(AX - BY)/(A^2 + B^2), \tag{1}$$

where

$$A = \omega\left[\gamma_1\left(\omega_2^2 - \omega^2\right) + \gamma_2\left(\omega_1^2 - \omega^2\right) - 2(\omega_1\omega_2)^{1/2}\Gamma_{12}\Delta_{12}\right],$$

$$B = \left(\omega_1^2 - \omega^2\right)\left(\omega_2^2 - \omega^2\right) + \omega^2\left(\Gamma_{12}^2 - \gamma_1\gamma_2\right) - \omega_1\omega_2\Delta_{12}^2,$$

$$X = F_1^2(\omega_2^2 - \omega^2) + F_2^2(\omega_1^2 - \omega^2) - 2F_1F_2(\omega_1\omega_2)^{1/2}\Delta_{12},$$
$$Y = \omega(F_1^2\gamma_2 + F_2^2\gamma_1 - 2F_1F_2\Gamma_{12}).$$

In this equation $n(\omega)$ is the Bose factor, $\omega_{1,2}$ are the TA and TO phonon frequencies, $\gamma_{1,2}$ are the phonon linewidths, and $F_{1,2}$ are the dynamic structure factors. Factoring out F_1^2 allows rewriting Eq. (1) in terms of the ratio F_2/F_1, thus reducing the number of fitting parameters by one. Δ_{12} and Γ_{12} are, respectively, the harmonic and the dissipative coefficients coupling the two modes. Most if not all the authors who have used the MC model to describe their phonon spectra have chosen to retain only one of these two coefficients and to set the other one to zero. Barker *et al.* [28] have shown that the two descriptions are mathematically equivalent through a unitary transformation. Because of this mathematical indeterminacy, the justification for using either harmonic (real) or dissipative (imaginary) coupling in the analysis of a given spectrum must be based on physical arguments, e.g., temperature or q dependence. We should also note that the expression for X in Eq. (1) is simplified, assuming that the two dynamic structure factors F_1 and F_2 have the same phase. A more general expression should include a $\cos\phi$ factor, in which ϕ is the phase angle between the two complex structure factors. As pointed out in by Eijt *et al.* [27], not only are the dynamic structure factors complex quantities which can differ from one zone to another but, in addition, the nature of the coupling (real vs imaginary) imposes a strict phase relation between the two eigenvectors. As a result, the sign of the coupling terms can be either positive or negative. In the fitting procedure we have considered these different possibilities, real vs imaginary coupling and positive vs negative coupling terms, and are making a determination based on the quality of the fits and especially on the physical validity of the values obtained for the fitting parameters. Because the instrumental resolution was much narrower than the observed full width at half maximum (FWHM) of the inelastic peaks [see the horizontal bar in the bottom panel of Fig. 4(a)], no resolution convolution was needed in fitting the data. In the (002) zone, the better fits by far were obtained assuming real coupling, as is usually the case for low frequencies and therefore low q since the coupling term for imaginary coupling is a function of ω [27,29]. In Figs. 3(b) and 3(d) the coupling constant is seen to be finite at $q = 0.05$ and 0.1 but zero at $q = 0.15$ below 800 K.

The mode coupling analysis was further extended to all q values in the (002) Brillouin zone. Since the temperature variations were found to be small (Figs. 2 and 3), the results are only shown for 723 K as representative of the temperature range studied across the 800 K transition. The fitted spectra and the phonon dispersion relations are shown in Fig. 4 and the values of the fitting parameters listed in Table I. The TO mode is found to be soft and overdamped at $\xi = 0.05$ and 0.1 and underdamped at larger q, while the TA mode is underdamped at small q but becomes overdamped near the zone boundary. As mentioned earlier, the TO mode is not clearly identifiable at $\xi = 0.1$ and not at all at $\xi = 0.05$. In addition, the intensity of the single peak, most certainly the TA mode, is nearly an order of magnitude larger at $\xi = 0.05$ than at $\xi = 0.1$. These observations do seem to point to a transfer of energy from the TO to the TA mode. At large q the two phonons are resolved and well separated and therefore noninteracting. Accordingly, the coupling constant Δ_{12} is found to be zero for larger q.

Complementary to the above constant q scans measurements, constant E scans were also made in the (002) zone at low energies. Such E scans can be particularly informative when the phonon peaks become very broad and overlapping in the constant q spectra, as in the present case with the TO and TA peaks. These scans were performed for fixed energy transfers from 3 to 10 meV and are presented in Fig. 4(c). The peaks were fitted with Gaussian function to determine the q peak position of the phonon mode for each energy transfer.

The fitting results of both constant q and constant E scans were used to map out the phonon dispersion in the [110] direction (Σ_4) as shown in Fig. 4(d). The vertical bar on each point of the curve represents the FWHM of the phonon peak at that q value. The TA phonon energy rises linearly at small q, then goes through a cusp at $q = 0.15$ and finally decreases toward 5 meV at the zone boundary. Between $\xi = 0.1$ and $\xi = 0.15$ the TO branch drops precipitously into the TA branch. This corresponds to the so-called waterfall phenomenon discussed in the Introduction. Constant E scans allowed us to follow the TO branch to its very intersection with the TA branch. Also noteworthy is the sudden increase of the TO mode FWHM at $\xi = 0.1$. A large FWHM that is increasing with q is a characteristic that is commonly observed in other relaxors displaying a waterfall feature, but it only represents an inhomogeneous broadening of the TO mode due to the particular shape of the TO phonon dispersion curve rather than dissipation and energy loss. The sharp drop of the TO branch can also explain the absence of a well defined soft TO mode intensity below q_{wf}. At higher q, the TO phonon energy increases continuously and reaches ~18 meV at the zone boundary, while the TA phonon energy decreases slightly toward the zone boundary. A recent study of $NaNbO_3$ by Tomeno *et al.* [30] reveals a similar behavior of the Σ_4 TO and TA phonons, although the TA mode in $NaNbO_3$ does not soften toward the zone boundary as it does here in NBT. It is also worth noting that the energy of the Σ_4 TA mode at the zone boundary is significantly lower in NBT than in nonrelaxor perovskite oxides such as $SrTiO_3$, $NaNbO_3$, and $KMnF_3$ [30–32] in which the rotation of the O_6 octahedra leads to the softening of the Σ_3 transverse acoustic branch toward the M point of the Brillouin zone. The eigenmode analysis [33] indicates that the M point zone boundary mode of the Σ_4 line consists of antiparallel displacements of the A site atoms (Na/Bi) along the cube edge in two adjacent columns along a cubic axis. The softening of the Σ_4 mode toward the M point may therefore suggest a partial correlation of the A site cation off-centering, a suggestion confirmed by neutron diffraction [15].

B. [001] phonon near (220) zone

We have also studied the TO and TA phonons in the orthogonal direction, i.e., propagating in the [001] direction and polarized in the [110] direction (Δ_5 in symmetry notation), with a similar set of constant q scans. The (220) spectra are shown in Fig. 5 near zone center (a) and at larger q toward the zone boundary (b). At small q, the (220) spectra are very similar to the (002) ones, except for the observation of a TO mode below

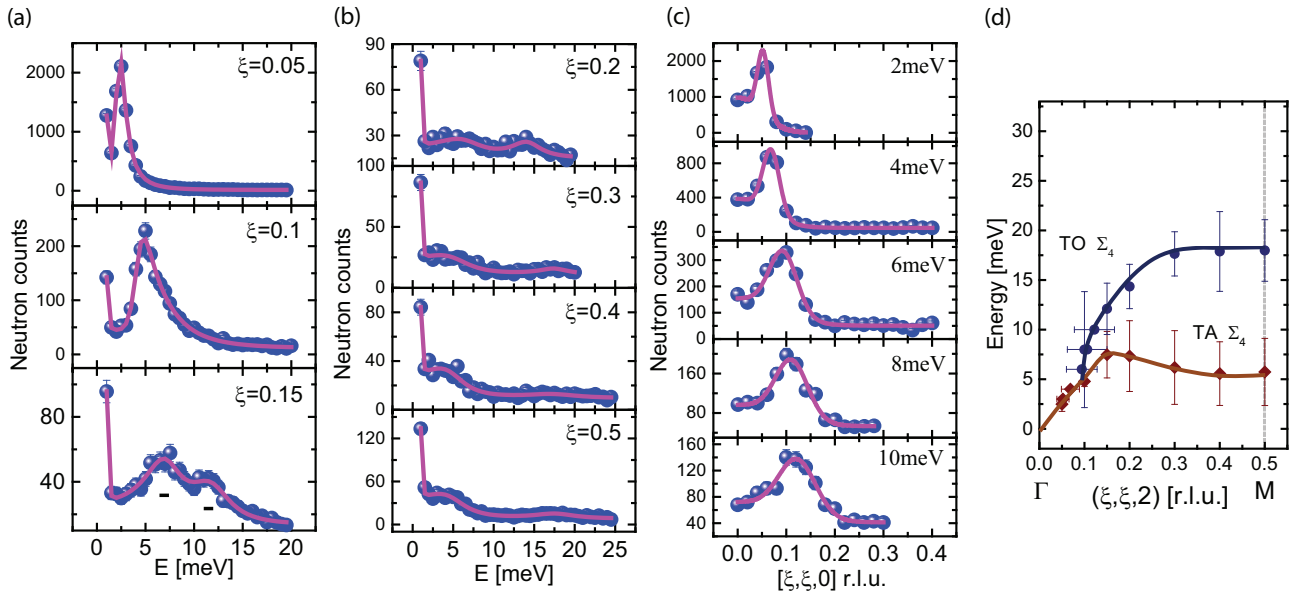

FIG. 4. (Color online) (a) and (b) Constant q scans of the [110] phonon at 723 K. The magenta lines are the fitted result as described in the text. We also show a set of constant E scans in (c). The dispersion relations in (d) are obtained from fitting to both constant Q and constant E scans. The vertical bars represent the FWHM of the peak. The solid lines in (d) are guides for the eye.

10 meV at the (220) zone center in Figs. 6(a) and 6(b), which is absent near or at the (002) zone center in Fig. 2(a). At large q however, the (220) spectra appear to be very different, with features that are much broader and more strongly overlapping than those in the (002) spectra, suggestive of a different type of coupling mechanism between the TO and TA phonons. In this (220) zone, the line shapes and energies of the modes do not vary significantly with temperature as shown in Fig. 5 and the spectra were therefore fitted and analyzed at 873 K.

To obtain the dispersion relation of the TO and TA phonon modes propagating in the [001] direction and polarized in the [110] direction, the same MC fitting model as in the (002) zone was successfully used. At small q and small frequencies, the (220) spectra were fitted assuming real coupling, as was done for the small q spectra in the (002) zone on account of the previously indicated ω dependence of the imaginary coupling term. Fitting assuming imaginary coupling was also attempted but was unsuccessful. At larger q ($\xi \geqslant 0.2$), similarly good fits of the spectra could be obtained assuming either real or imaginary coupling, in both cases with opposite signs for F_2/F_1 and Δ_{12} or Γ_{12} (negative coupling term). It is important to reiterate that, although good fits can be obtained with either choice of coupling, these result in two different sets of fitted values of the parameters. The data points and fitted curves are shown in Fig. 6(c) and the dispersion curves are shown in Figs. 6(d) and 6(e) for real and imaginary coupling,

TABLE I. Fitting parameters for the MC model.

BZ	Q	ω_{TA} (meV)	γ_{TA} (meV)	ω_{TO} (meV)	γ_{TO} (meV)	Δ_{12} (meV)	Γ_{12} (meV)	F_2/F_1
(002)	(0.05, 0.05, 2)	2.21	0.50	2.89	5.96	1.79	0	1.39
	(0.1, 0.1, 2)	4.78	0.94	7.99	11.70	3.22	0	1.55
	(0.15, 0.15, 2)	7.48	4.68	12.10	5.18	0	0	1.41
	(0.2, 0.2, 2)	7.34	7.18	14.40	4.75	0	0	1.58
	(0.3, 0.3, 2)	6.41	7.94	17.80	5.53	0	0	1.41
	(0.4, 0.4, 2)	5.50	6.47	19.30	12.80	0	0	1.43
	(0.5, 0.5, 2)	5.78	6.91	18.30	7.51	0	0	1.57
(220) Real	(2, 2, 0.1)	3.82	0.76	7.37	9.66	2.43	0	0.75
	(2, 2, 0.2)	11.06	2.92	9.24	8.53	4.06	0	− 2.46
	(2, 2, 0.3)	13.11	2.96	11.90	19.60	6.43	0	− 2.44
	(2, 2, 0.4)	14.93	2.42	15.60	27.40	9.72	0	− 2.60
	(2, 2, 0.5)	16.10	2.40	16.30	29.30	10.85	0	− 2.83
(220) Imaginary	(2, 2, 0.2)	8.02	9.05	11.16	3.00	0	8.52	− 2.35
	(2, 2, 0.3)	8.85	14.71	14.12	6.39	0	12.96	− 2.40
	(2, 2, 0.4)	8.87	13.88	19.11	14.30	0	16.28	− 2.50
	(2, 2, 0.5)	8.95	13.79	25.65	25.2	0	17.75	− 2.63

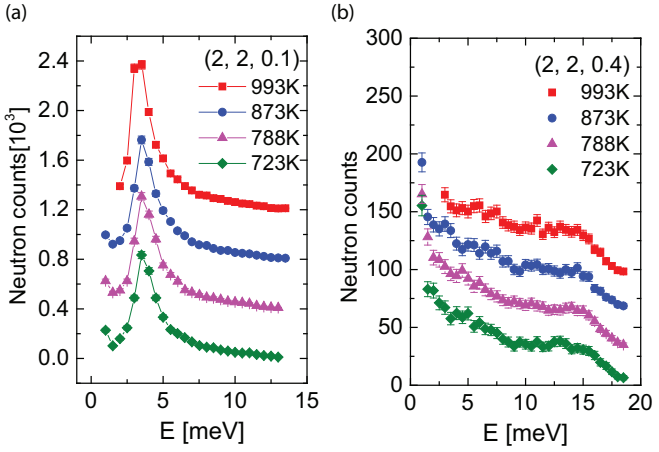

FIG. 5. (Color online) Temperature overplots of constant q scans at (a) near zone center (2, 2, 0.1) and (b) near zone boundary (2, 2, 0.4). The spectra between temperatures are offset by a constant for clarity.

respectively. On the dispersion curves, the points mark the bare phonon frequencies obtained from the model fit. The values of the fitting parameters are listed in the second part of Table I for both real and imaginary coupling. With real coupling, the bare frequencies of both modes fall within the measured spectral intensity, the TO mode is increasingly overdamped with q but the TA mode remains underdamped, more directly reflecting the raw spectral behavior. The two phonon branches become very close or even cross between $\xi \geqslant 0.2$, which is where the goodness of fit imposes that the sign of the ratio F_2/F_1 be changed to negative. The coupling constant shown in the inset of Fig. 6(d) also exhibits a regular behavior, replicating the shape of the dispersion curves. With imaginary coupling, both modes are overdamped, the bare TO frequency falls well outside the measured spectral intensity and is much higher than the frequency of the TA mode which is suppressed. In order to couple the two modes and properly fit the measured spectra, the coupling constant must then be made to exceed the frequency of the phonon themselves, casting doubt on even the validity of two separate bare phonons. Based on the fitted values of the parameters, the dispersion behavior and the above considerations, the real coupling version of the MC model appears to be better justified than the imaginary one. Such a choice is also supported by complementary measurements of NBT made in the same conditions [34]. These show the two phonon branches almost overlapping. Note that the phonon mode energies below $\xi = 0.1$ are estimated from spectral intensity, and the dispersion curves are extrapolated from higher q. Therefore, the difference in the zone center TO phonon behavior as indicated by the dispersion curves in Figs. 4(d) and 6(d) may be overestimated. In addition, the large q spectra in Fig. 6(a) show a remarkable resemblance with those at constant q in $BaTiO_3$ (Fig. 4 in Ref. [29]), a system in which a real coupling model was used, resulting in a similar crossing of the two [001] phonon branches of the phonons. Similar dispersion curves to these obtained in NBT have also been reported by Eijt *et al.* for the $Sn_2P_2Se_6$ system [27], which were also described assuming real coupling. Finally, this choice can also be justified on the basis of the physical considerations proposed in the next section.

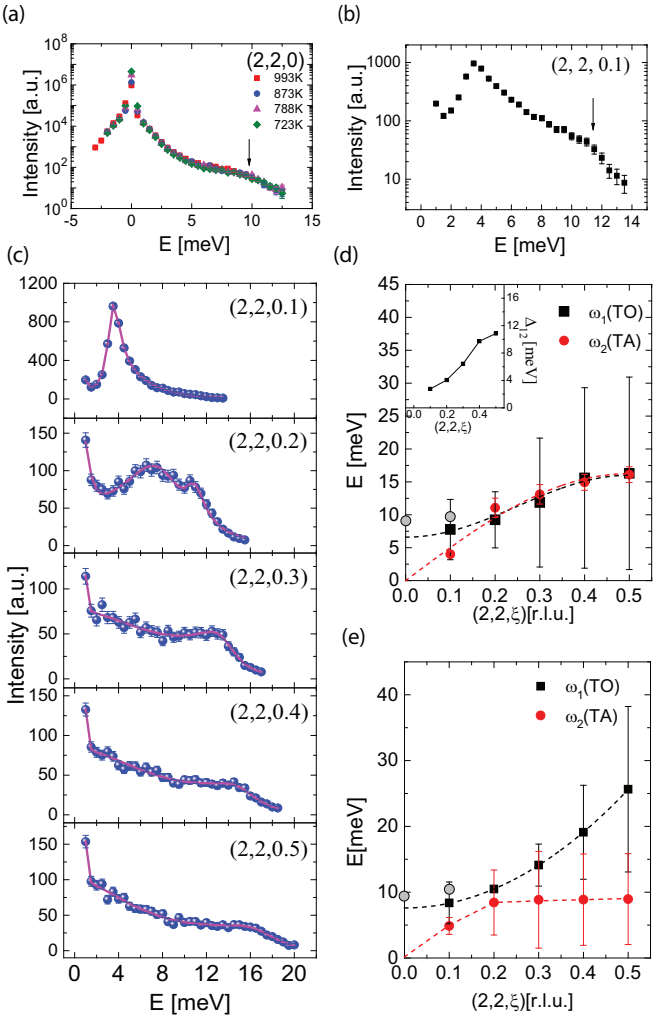

FIG. 6. (Color online) (a) (2, 2, 0) and (b) (2, 2, 0.1) constant q scans plotted in log scale. (c) (2, 2, q) phonons measured in constant q mode at 873 K and fitted with the MC model. Phonon dispersion relation obtained by assuming real coupling (Δ_{12}) and imaginary coupling (Γ_{12}) are shown in (d) and (e), respectively. The inset in (d) shows the real coupling constant Δ_{12} as function of q. The solid gray circles are apparent spectral intensities at (2, 2, 0) and (2, 2, 0.1). The dashed lines are guides for the eye, see text for explanation.

IV. DISCUSSION

The key features of the two sets of inelastic scans presented can be summarized as follows: (i) In the (002) zone along the Σ_4 branch, the TO phonon exhibits a precipitous drop or waterfall in the vicinity of (0.1, 0.1, 2) and is no longer identifiable below. The TA mode is underdamped throughout the Brillouin zone and rapidly increases in intensity with decreasing q. (ii) In the (220) zone along the Δ_5 branch, the TO phonon intensity is still observed near the zone center, hence the waterfall effect is either suppressed or absent. At larger q, the TO and TA phonon overlap significantly and therefore remain strongly coupled throughout the (220) zone, even more so in the case of real coupling. The mode coupling model was found to be more adequate describing our data than the individual damped harmonic oscillator model, particularly in the small q region. This is because the two phonon modes in

both Brillouin zones are overdamped and largely overlapping. However, at large q in the (002) zone, the TA and TO phonons are well separated and underdamped. As a result, the coupling constant in MC fitting is essentially zero for near (002) zone boundary spectra. In this regard, the MC model is not superior to the individual harmonic oscillator model in the large q region. Therefore, whether or not the mode coupling model is appropriate in describing the phonon data depends on the individual mode character and its relation with the neighboring phonon mode.

In the following we first discuss the significance of the MC model in describing the neutron spectral data and then examine the differences in phonon behavior between the two zones, first near the zone center and second near the zone boundary.

A. The presence of waterfall feature in the (002) zone

The fact that a waterfall feature is observed in the (002) zone but not in the (220) zone may be surprising at first since the phonons are the same in cubic symmetry in the limit of $q = 0$, i.e., at the zone center. It is therefore necessary to examine the values of the fitting parameters to understand the cause of the different phonon behaviors in the two zones. As pointed out by Hlinka *et al.* [20] and others, a waterfall feature might be observed in certain zones and not in others since the dynamical structure factors and therefore the coupling term in Eq. (1) can vary between zones (the $\mathbf{Q}^2$ dependence). However, different behaviors can also be explained by varying degrees of overlap of the phonons or different coupling mechanisms and values of the coupling parameter. As seen in Table I, the coupling constant in the (220) zone is only 2/3 that in the (002) zone and the overlap between the two modes at small q is also much smaller. In addition, two physical considerations may be determinant in explaining the absence or suppression of a waterfall feature in the (220) zone. First, we note that the high temperature transition in NBT corresponds to an in-plane cog wheel-type rotation of the oxygen octahedra that leads to (a) a doubling of the unit cell and, more importantly, (b) a rotation of the crystal axes by 45°, similar to that in the systems mentioned previously, $SrTiO_3$, $NaNbO_3$, and $KMnF_3$. As a result, the new horizontal axes now lie along the ⟨110⟩ cubic directions while the tetragonal c axis is still along a cubic ⟨001⟩ direction. Second, in NBT this rotation of octahedra is accompanied by cation displacements along the c axis [15], resulting in the formation of polar nanodomains (PNDs), the reorientation of which gives rise to the relaxor behavior below ∼900 K [12]. The PNDs, being polar and therefore without inversion symmetry, are also piezoelectric. This fact was recently shown to explain the electroacoustic resonances observed in the relaxor $K_{1-x}Li_xTaO_3$ (KLT) [13]. These two physical considerations and the piezoelectric nature of the PNDs may explain the observation of a waterfall effect in the (002) zone at small q. In this zone indeed, the TO mode is polarized along the c axis and can directly modulate the PND polarization while the propagation direction of the phonons along the pseudocubic ⟨110⟩ direction ensures the transverse piezoelectric coupling to strain. In such a scenario, the piezoelectric coefficient defined in terms of the new axes would be d_{34} or d_{35}, coupling the local polarization component P_3, with the product of the atomic displacements u_3u_2 or u_3u_1. The existence of a piezoelectric interaction between optic and acoustic phonons was already proposed very early by Dvorak [35] to explain the TO-TA coupling in tetragonal $BaTiO_3$, although in this case the piezoelectric character was simply an intrinsic attribute of the ferroelectric phase. In the same tetragonal $BaTiO_3$, Fleury and Lazay demonstrated the piezoelectric nature of the coupling between an overdamped optic mode and an underdamped acoustic mode [36]. They reported a greatly enhanced Brillouin scattering cross section that was strongly dependent on phonon polarization and propagation direction. Now considering the particular wave vector q_{wf}, at which the waterfall feature is observed, only phonons with wavelengths that are greater than the average size of PNDs or a wave vector $q \leqslant q_{wf}$ can coherently modulate their polarization. For phonon wavelengths greater than the typical size of a PND or wave vectors smaller than q_{wf}, the polarizations of an increasing number of PNDs can be simultaneously and therefore coherently modulated by the TO phonon, the energy of which is then piezoelectrically transferred to the TA phonon. This can explain why the TO phonon first broadens and is then no longer observed for $\xi < 0.1$, while the intensity of the TA mode increases rapidly below $\xi = 0.15$. This interpretation might seem to be contradicted by the smaller fitted value of the coupling coefficient obtained at (0.05, 0.05, 2) than at (0.1, 0.1, 2) in Table I. However, the assumption of two coupled independent modes is expected to no longer be valid for strong piezoelectric coupling below q_{wf}.

A description of mode coupling was proposed early on by Fano to describe the interaction between a discrete state or configuration and a continuum of configurations, leading to an admixture state and resulting in characteristically asymmetric spectral line shapes [37]. This does seem to correspond to the present NBT case in which the TO phonon can decay into a continuum of long wavelength polarization fluctuations and piezoelectrically transfer its energy to the TA phonon. In Fano's model, the spectral density is expressed as

$$I(\omega) = \frac{(Q+\epsilon)^2}{1+\epsilon^2}, \tag{2}$$

where $\epsilon = \frac{\omega-\omega_0}{\Gamma}$ is the reduced energy, Γ is the spectral width of the discrete excited state, and the Fano Q is a modified coupling constant which incorporates the ratio of the transition probabilities, respectively, to the admixture state and to the unperturbed continuum state. The fitted curves in Fig. 7 show a good match between the Fano line shape and our data. The two spectra are taken at small q values where the coupling is the strongest. The values of the parameters are given in Table II. As expected, the Fano coupling constant Q is more than three times larger and the width Γ less than half at $\xi = 0.05$ than it is at $\xi = 0.1$, demonstrating that the coupling of the two modes is much stronger or their hybridization much more complete at the lower q.

If the phonon spectra appear similar at small q in the (002) and in the (220) zone, apart from the absence of waterfall in the latter, they are very different at larger q and close to the zone boundary. In the (002) zone past q_{wf}, the TO mode energy increases up to approximately 18 meV where it is underdamped and therefore well separated from the TA

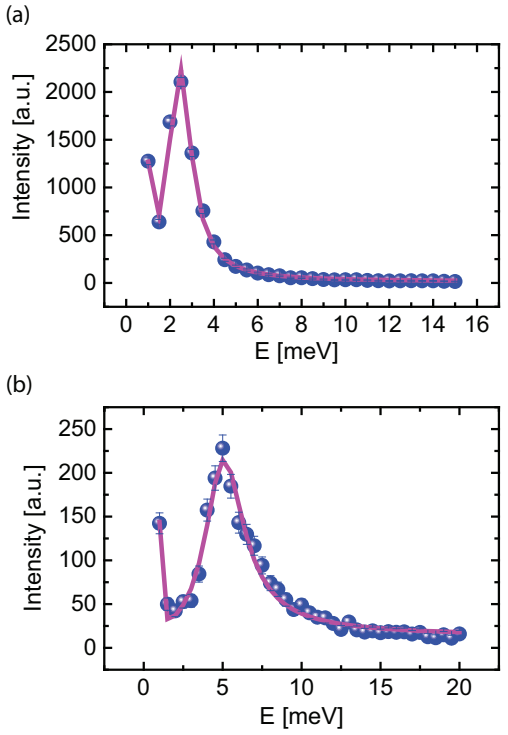

FIG. 7. (Color online) Data and fitted curve of Eq. (2) for constant q scan at (a) (0.05, 0.05, 2) and (b) (0.1, 0.1, 2). The fitting parameters are shown in Table II.

mode. However, the TA mode displays an unusual frequency dependence, going through a cusp at $\xi = 0.15$ and decreasing to an energy of 5 meV at the boundary. This softening was discussed earlier in Sec. III A as reflecting a second order coupling between the antiphase cation displacements and rotations of the oxygen octahedra.

B. Phonon anisotropy in the (220) zone

As noted at the beginning of this section, the low q spectra in the (220) zone differ from those in the (002) zone by the observation of a TO mode. The waterfall feature is therefore absent or suppressed in that zone. At larger q, the (220) spectra are quite different from the (002) ones and, although still well described by the MC model with real coupling, they yield very different dispersion curves for the bare phonons. Given the presence of polar nanodomains and their likely role in coupling the phonons, this difference can also be attributed to a coupling anisotropy between the two zones. In the (220) zone, the TO phonon propagates in the c direction and is polarized in a ⟨110⟩ direction. Such a phonon cannot modulate the PND polarization as effectively as in the other zone (as supported by the respective values of the TO damping coefficient listed in Table I at $q = 0.2$). Moreover, the cog-wheel rotations of the octahedra, accompanying cation displacements and resulting strain are correlated in-plane but not out-of-plane. Therefore, in the (220) zone the coupling between polarization and strain corresponding the TO-TA interaction is likely not coherent. This anisotropy in the phonon coupling may be further amplified by a chemical distribution of Bi and Na in alternating planes along a single cubic direction [38].

In the (220) zone, a satisfactory fit of the spectrum at $q = 0.1$ could only be obtained assuming real coupling and a positive ratio of the dynamical structure factors F_2/F_1. At larger q, satisfactory fits could be obtained assuming either real or imaginary coupling but with a negative sign for the ratio F_2/F_1 in either case. As indicated in the results section, based on the values of the fitted parameters and the shape of the dispersion curves, real coupling is deemed more physical. However, it is interesting to note that the value of the ratio was found to be approximately the same for both choices. As discussed below Eq. (1), the sign change for $\xi > 0.1$ should reflect a relative phase change between the two complex structure factors. It may be meaningful to note that this sign change occurs at a q value where the two branches become extremely close.

TABLE II. Fitting parameters for phonon spectra at (0.05, 0.05, 2) and (0.1, 0.1, 2) to the Fano model.

Parameters	(0.05, 0.05, 2)	(0.1, 0.1, 2)
ω_0 (meV)	2.43	4.94
Γ (meV)	0.65	1.50
Fano Q	33.42	10.08

V. SUMMARY AND CONCLUSION

In summary, we have reported measurements of the low energy transverse optic and acoustic phonons of $Na_{1/2}Bi_{1/2}TiO_3$ (NBT) in two different zones, (002) and (220), in the $[H\,H\,L]$ scattering plane and in a 200 K temperature range around the higher temperature transition $T_c \simeq 820$ K. The results reveal a significant anisotropy in the phonon coupling and damping between the two orthogonal directions. The phonons are found to be coherently coupled at small q, but more strongly in the (002) zone than in the (220) zone. In the (002) zone, the TO phonon branch falls precipitously into the TA branch at $q_{wf} \sim 0.14$ r.l.u. (waterfall) and is no longer observed at smaller q. This is interpreted as a hybridization of the two phonon modes which are (real) coupled via the piezoelectric polar nanodomains (PNDs) that are known to be present in this temperature range. Accordingly, the intensity of the TA phonon is seen to increase by an order of magnitude. This coupling is reinforced by the rotation of the lattice axes resulting from the in-plane cog-wheel rotation of the oxygen octahedra. At intermediate q, the TA mode exhibits a cusp and is slightly depressed toward the zone boundary, due to what appears to be an indirect coupling of its eigenmode to rotations of the oxygen octahedra. At small q in the (220) zone, the TO-TA coupling is 30% weaker than in the other zone and no waterfall is observed. This is tentatively attributed to the incoherent out-of-plane coupling of octahedra and accompanying cation displacements between layers. At larger q, the dispersion curves cross but the bare phonons overlap extensively over most of the Brillouin zone possibly due to coupling via short wavelength polarization fluctuations

(within PNDs). Similarities in the phonon spectra of NBT, $NaNbO_3$ and even $BaTiO_3$ are noted, which can be traced to the existence of local polar order in these systems, although much more developed in NBT. The similarity between the dispersion curves obtained in NBT and $Sn_2P_2Se_6$ also suggests that coupling between phonons should be a general feature of systems in which local order develops before long range order is established.

ACKNOWLEDGMENTS

We thank D. Viehland for suggesting this study of NBT and are grateful to P. Gehring, S. Vakhrushev, and B. Hennion for helpful discussions. The neutron scattering experiments conducted at ORNL's High Flux Isotope Reactor were sponsored by the Scientific User Facilities Division, Office of Basic Energy Sciences, U.S. Department of Energy.

[1] Y. Hiruma, H. Nagata, and T. Takenaka, J. Appl. Phys. **105**, 084112 (2009).
[2] J. Suchanicz, J. Mater. Sci. **37**, 489 (2002).
[3] M. Matsuura, H. Iida, K. Hirota, K. Ohwada, Y. Noguchi, and M. Miyayama, Phys. Rev. B **87**, 064109 (2013).
[4] W. Ge, C. P. Devreugd, D. Phelan, Q. Zhang, M. Ahart, J. Li, H. Luo, L. A. Boatner, D. Viehland, and P. M. Gehring, Phys. Rev. B **88**, 174115 (2013).
[5] R. A. Cowley, Phys. Rev. **134**, A981 (1964).
[6] V. J. Minkiewicz and G. Shirane, J. Phys. Soc. Jpn **26**, 674 (1969).
[7] A. M. Glazer and H. D. Megaw, Acta Crystallogr. Sect. A **29**, 489 (1973).
[8] G. O. Jones and P. A. Thomas, Acta Crystallogr. Sect. B **58**, 168 (2002).
[9] J. Kreisel, P. Bouvier, B. Dkhil, P. A. Thomas, A. M. Glazer, T. R. Welberry, B. Chaabane, and M. Mezouar, Phys. Rev. B **68**, 014113 (2003).
[10] G. A. Samara, J. Phys.: Condens. Matter **15**, R367 (2003).
[11] J. Toulouse, B. E. Vugmeister, and R. Pattnaik, Phys. Rev. Lett. **73**, 3467 (1994).
[12] C.-S. Tu, I. G. Siny, and V. H. Schmidt, Phys. Rev. B **49**, 11550 (1994).
[13] J. Toulouse, L. Cai, R. K. Pattnaik, and L. A. Boatner, Europhys. Lett. **105**, 17001 (2014).
[14] A. M. Glazer, Acta Crystallogr. Sect. A **31**, 756 (1975).
[15] G. O. Jones and P. A. Thomas, Acta Crystallogr. Sect. B **56**, 426 (2000).
[16] P. M. Gehring, S. E. Park, and G. Shirane, Phys. Rev. Lett. **84**, 5216 (2000).
[17] P. M. Gehring, S. E. Park, and G. Shirane, Phys. Rev. B **63**, 224109 (2001).
[18] H. Cao, C. Stock, G. Xu, P. M. Gehring, J. Li, and D. Viehland, Phys. Rev. B **78**, 104103 (2008).
[19] C. Stock, P. M. Gehring, H. Hiraka, I. Swainson, G. Xu, Z.-G. Ye, H. Luo, J.-F. Li, and D. Viehland, Phys. Rev. B **86**, 104108 (2012).
[20] J. Hlinka and S. Kamba, Phase Transitions **81**, 491 (2008).
[21] S. B. Vakhrushev and S. M. Shapiro, Phys. Rev. B **66**, 214101 (2002).
[22] I. P. Swainson, C. Stock, P. M. Gehring, G. Xu, K. Hirota, Y. Qiu, H. Luo, X. Zhao, J. F. Li, and D. Viehland, Phys. Rev. B **79**, 224301 (2009).
[23] G. Shirane, S. M. Shapiro, and J. M. Tranquada, *Neutron Scattering With a Triple-Axis Spectrometer* (Cambridge University Press, Cambridge, UK, 2002).
[24] C. H. Perry, R. Currat, H. Buhay, R. M. Migoni, W. G. Stirling, and J. D. Axe, Phys. Rev. B **39**, 8666 (1989).
[25] C. Stock, H. Luo, D. Viehland, J. F. Li, I. P. Swainson, R. J. Birgeneau, and G. Shirane, J. Phys. Soc. Jpn. **74**, 3002 (2005).
[26] R. Currat, H. Buhay, C. H. Perry, and A. M. Quittet, Phys. Rev. B **40**, 10741 (1989).
[27] S. Eijt, R. Currat, J. E. Lorenzo, P Saint-Gregoire, S. Katano, T. Janssen, B. Hennion, and Y. Vysochanskii, J. Phys.: Condens. Matter **10**, 4811 (1998).
[28] A. S. Barker and J. J. Hopfield, Phys. Rev. **135**, A1732 (1964).
[29] J. Harada, J. D. Axe, and G. Shirane, Phys. Rev. B **4**, 155 (1971).
[30] I. Tomeno, Y. Tsunoda, K. Oka, M. Matsuura, and M. Nishi, Phys. Rev. B **80**, 104101 (2009).
[31] N. Lehner, H. Rauh, K. Strobel, R. Geick, G. Heger, J. Bouillot, B. Renker, M. Rousseau, and W. G. Stirling, J. Phys. C **15**, 6545 (1982).
[32] W. G. Stirling, J. Phys. C **5**, 2711 (1972).
[33] Eigenmode analysis were performed in SMODES from the ISOTROPY software suite, ISOTROPY (2013), http://stokes.byu.edu/iso/isotropy
[34] P. Ondrejkovic, J. Hlinka, M. Kempa, J. Kulda, H. Luo, and Q. Zhang, Phase Transitions **84**, 829 (2011).
[35] V. Dvorak, Phys. Rev. **167**, 525 (1968).
[36] P. A. Fleury and P. D. Lazay, Phys. Rev. Lett. **26**, 1331 (1971).
[37] U. Fano, Phys. Rev. **124**, 1866 (1961).
[38] M. Gröting, S. Hayn, and K. Albe, J. Solid State Chem. **184**, 2041 (2011).